Electronic Supplementary Material (ESI) for Soft Matter.

Supplementary Information

Correlation between morphology and anisotropic transport properties of diblock copolymers melts

Mohammed Suliman Alshammasi and Fernando A. Escobedo*

Robert Frederick Smith School of Chemical and Biomolecular Engineering, Cornell University,
Ithaca, NY 14853, USA

I) Details of Simulated Systems

Details about the simulation box dimensions are shown in Table S1.

Table S1. Size and composition of simulated systems

N	Structure	A Beads	B Beads	x-dimension (σ)	y-dimension (σ)	z-dimension (σ)
10	**Lamellae**	2,560	2,560	18.3	18.3	18.3
14		5,040	5,040	22.8	22.8	22.8
24		14,688	14,688	32.6	32.6	32.6
32		3,216	3,216	19.7	19.7	19.7
40		5,040	5,040	22.8	22.8	22.8
50		7,850	7,850	26.4	26.4	26.4
64		12,706	12,706	31.1	31.1	31.1
76		17,842	17,842	34.9	34.9	34.9
200		5,000	5,000	13.3	13.3	66.0^{a}
14	**Cylinder**	8,160	29,920	35.5	35.5	35.5
24		1,920	5,760	20.8	20.8	20.8
40		2,300	6,900	22.1	22.1	22.1
60		3,720	11,160	26.0	26.0	26.0
18	**Gyroid**	7,998	15,996	30.4	30.4	30.4
40	**Sphere**	880	7,920	21.8	21.8	21.8
10	**Homopolymer**	5,120	–	18.3	18.3	18.3
14		10,080	–	22.8	22.8	22.8
24		29,376	–	32.6	32.6	32.6
40		10,080	–	22.8	22.8	22.8
64		25,412	–	31.1	31.1	31.1
76		35,684	–	34.9	34.9	34.9
100		10,000	–	22.7	22.7	22.7
150		10,500	–	23.1	23.1	23.1

[a] z-direction is normal to the interface.

II) Finite-Size Effect Analysis

Self-diffusion coefficient (D) is the most susceptible property to system size.[1] Table S2 illustrates the effect of system size (i.e., number of domains) for diblock copolymer with Lamellae morphology on D for chain lengths $N = 10$ (Rouse regime) and $N = 32$ (reptation regime). The results indicate that finite-size effects are minimal, leading to a slight but consistent increase in the D values, in agreement with previous studies.[2,3]

Table S2. Effect of number of lamellae domains on D for two chain lengths.

Number of Domains	$\boldsymbol{N = 10}$	$\boldsymbol{N = 32}$
1	$-$	$0.0028 \pm 0.0002\ \sigma^2/\tau$
2	$0.014 \pm 0.001\ \sigma^2/\tau$	$0.0035 \pm 0.0002\ \sigma^2/\tau$
4	$0.016 \pm 0.001\ \sigma^2/\tau$	$-$

III) Cox-Merz Rule Applicability

One method to check if the strain amplitude (γ_0) used in oscillatory shear dynamics results in a linear response behavior is by testing the validity of the Cox-Merz Rule. The Cox-Merz Rule is an empirical rule which states that the dependence of the steady shear viscosity (η) on the shear rate ($\dot{\gamma}$) is equivalent to the dependence of the complex viscosity (η^*) on the oscillation frequency (ω).[4]

In our oscillatory shear dynamics simulations, γ_0 was fixed to 10%. As shown inf Figure S1, for chain length $N = 40$, in the perpendicular ($L \perp$) and parallel ($L \parallel$) orientations, the Cox-Merz Rule applies indicating that values from our oscillatory shear dynamics simulations are derived from the linear response regime.

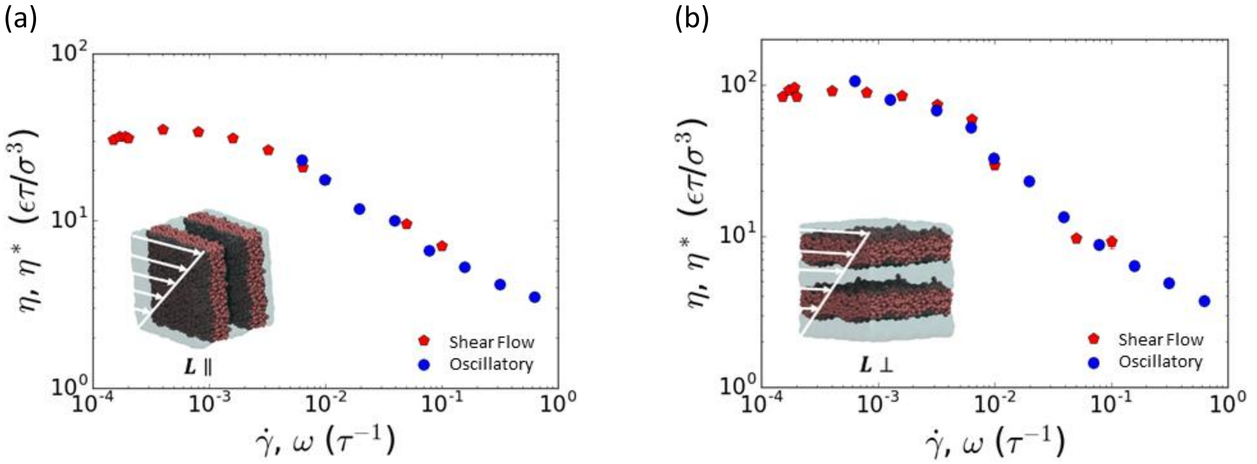

Figure S1. The dependence of η on $\dot{\gamma}$ and η^* on ω for a DBP with $N = 40$ at $T = 2.63\ \epsilon/k_b$ for two flow orientations as indicated in the inset.

IV) Self-Diffusion Coefficient and Zero-Shear Viscosity Mapping to Polyethylene

One method of determining if the oscillatory (and simple) shear simulations are performed for a wide-enough ω (and $\dot{\gamma}$) range to probe experimentally relevant time scales, is to obtain the zero-shear steady viscosity (η_0) and dynamic viscosity (η_0^*) to confirm that the Newtonian regime is approached. Figure S1 showed that this was indeed the case, hence indicating that the range used in this study is sufficient to capture the different relaxation modes of the melt.

Moreover, one can map the results obtained from coarse-grained simulations conducted in reduced units into data in real units for specific polymers for which experimental or atomistic simulation results are known, and thus check the level of agreement between the results. By doing so, one also obtains values for the characteristic mass (m), time (τ), length (σ), and energy (ϵ). We mapped our results for D to experimental and atomistic simulations data for linear polyethylene melts[5–8] (Figure S2) by matching the crossover molecular-weight (M_c) of the self-diffusion coefficient (D) from the Rouse to reptation scaling and the relevant density of the polymer (ρ) and temperature of the experiment (T). Table S3 lists the characteristic quantities being mapped. Using these quantities, Figure S3 shows that η_0 results from our simulations are also in good agreement with experimental data of polyethylene.

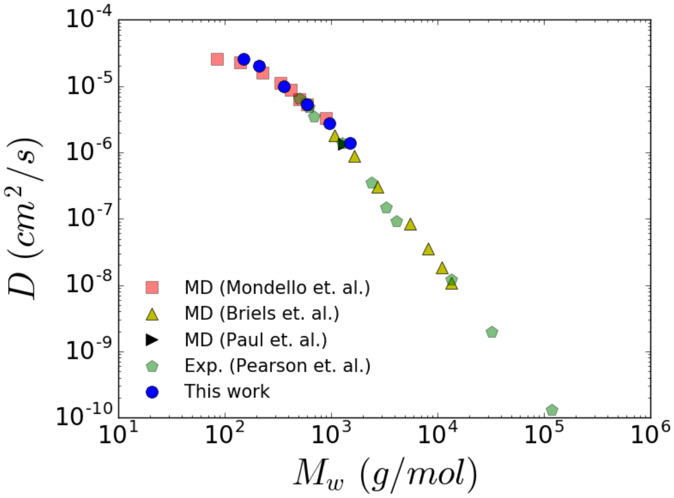

Figure S2. Simulation results for D from this work mapped to polyethylene using conversion Table S3. Data from experiments and atomistic simulations are superimposed.

Table S3. Mapping of characteristic quantities between KG model and polyethylene

System	ρ	T	M_c	m	ϵ	τ	σ
KG Model	$0.85\ \sigma^{-3}$	$2.63\ \epsilon/k_b$	60	1	1	1	1
Polyethylene[6]	$0.77\ g/cc$	$450\ K$	$600\ g/mol$	$10\ g/mol$	$1422\ J/mol$	$9.2 \times 10^{-13}\ s$	$3.5 \times 10^{-8}\ cm$

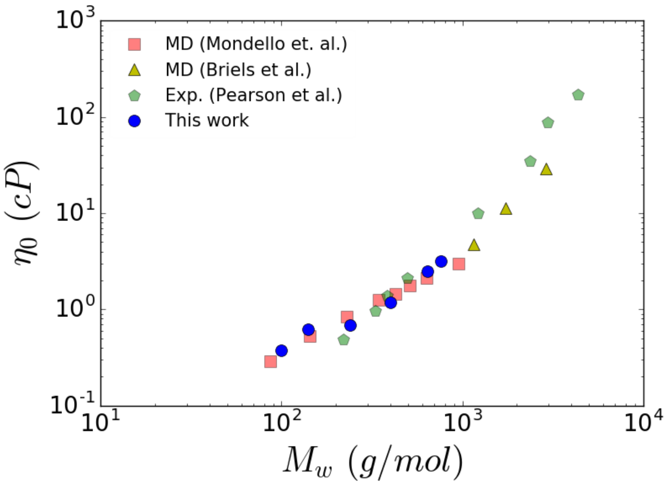

Figure S3. Simulation results of η_0 from this work compared to experimental and computational data for polyethylene using mapping of Table S3.

V) Uniaxial Deformation Simulations

The mechanical properties of polymeric materials can be characterized from their response to uniaxial deformation. In such experiments, a specimen is elongated in one direction, resulting in the simultaneous sample compression in the directions orthogonal to the elongation direction. Such experiments readily yield the Young's modulus (E), which is a measure of how stiff the material is. The stiffness typically increases for systems whose chains extend in the elongation direction.

To corroborate the argument given in the main text regarding the correlation between microscopic chain conformations and orientations and the macroscopic anisotropic viscosity, we performed uniaxial deformation simulations of the Lamellae (L) and Hexagonal Cylinder (HC) in the two distinct orientations (Figure S4) (i.e., parallel and perpendicular directions).

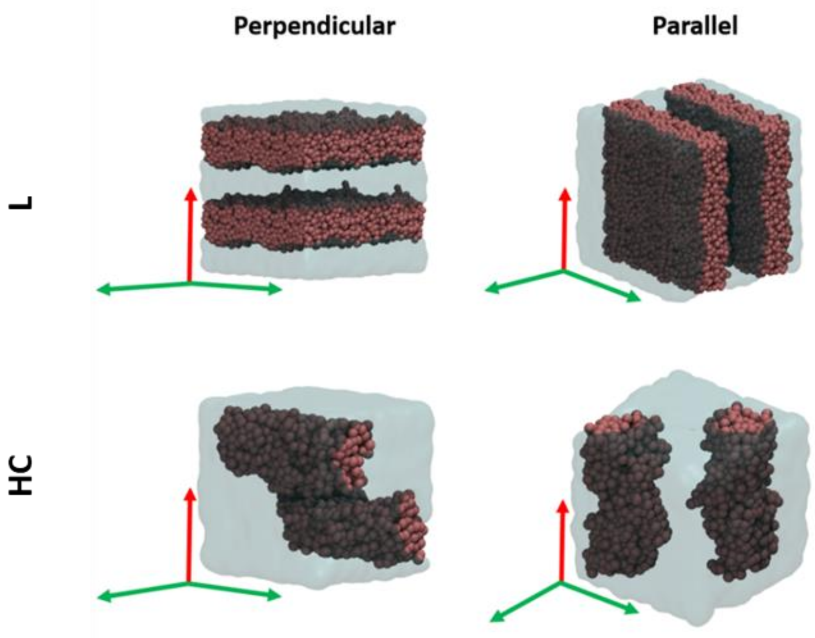

Figure S4. The different uniaxial flow directions possible for the L and HC morphologies, where the red arrow represents the extensional direction and the green arrows represent the compression directions.

For these simulations a deformation rate of $3.5 \times 10^{-5}\ \upsilon/\tau$ was used, where υ is the extension ratio defined as the ratio of the deformed dimension of the box to the initial undeformed state dimension. The stress (σ_{ii}^{*}) was calculated using eq. S1, where p_{ii} is the pressure tensor component in the direction of extension, p_{jj} (p_{kk}) is the pressure tensor component in the compression direction, and κ is the Possion's ratio, which is assumed to be 0.5 (a representative value of polymeric materials and appropriate for volume conserving incompressible material).[9]

$$\sigma_{ii}^{*} = -p_{ii} + \kappa\left(p_{jj} + p_{kk}\right) \qquad \text{(S1)}$$

E was calculated as the slope from the initial linear part of the stress—strain relation (Figure S5). In the perpendicular direction, chains in the L phase are more aligned in the elongation direction than chains in the HC phase, hence, E for the perpendicular L orientation is larger than that of the perpendicular HC orientation (Figure S6). In the parallel direction, both phases have similar E value since they have similar alignment (end-to-end distance distribution) in the elongation direction. These results are consistent with the analysis given in the main test regarding the effect of the chain conformations in the unperturbed state on the anisotropic viscosity trends.

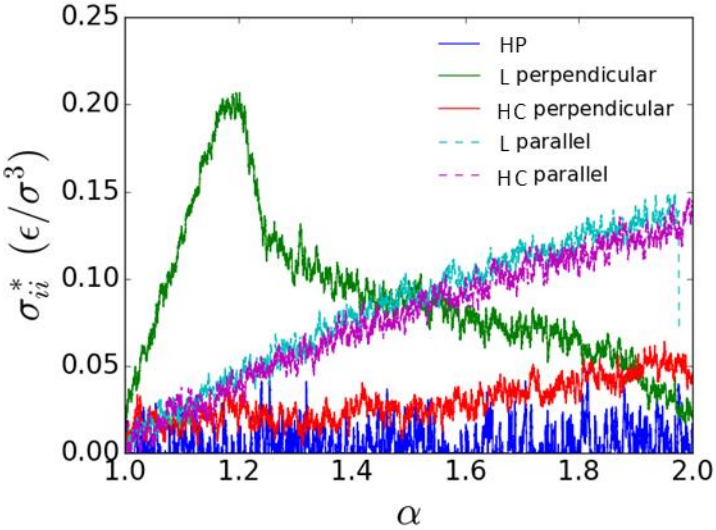

Figure S5. Stress—Strain relationship for DBPs with L and HC morphologies uniaxially deformed in the different possible directions (Figure S5) compared to the HP case for chain length $N = 40$ and $T = 2.6\ \epsilon/k_b$.

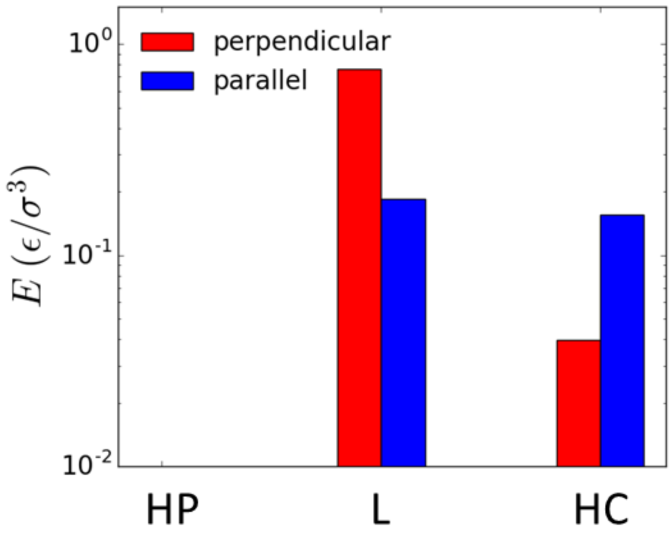

Figure S6. Young's modulus E obtained from uniaxial deformation for different morphologies having different orientations with respect to the elongation direction (as per Figure S3), for chain length $N = 40$ and $T = 2.6\ \epsilon/k_b$.

References

1 S. Sen, S. K. Kumar and P. Keblinski, *Macromolecules*, 2005, **38**, 650–653.
2 I.-C. Yeh and G. Hummer, *J. Phys. Chem. B*, 2004, **108**, 15873–15879.
3 A. Malevanets and J. M. Yeomans, *Europhys. Lett.*, 2000, **52**, 231–237.
4 W. P. Cox and E. H. Merz, *J. Polym. Sci.*, 1958, **28**, 619–622.
5 M. Mondello and G. S. Grest, *J. Chem. Phys.*, 1995, **103**, 7156–7165.
6 J. T. Padding and W. J. Briels, *J. Chem. Phys.*, 2002, **117**, 925–943.
7 W. Paul, G. D. Smith and D. Y. Yoon, *Macromolecules*, 1997, **30**, 7772–7780.
8 D. S. Pearson, G. Ver Strate, E. Von Meerwall and F. C. Schilling, *Macromolecules*, 1987, **20**, 1133–1141.
9 G. N. Greaves, A. L. Greer, R. S. Lakes and T. Rouxel, *Nat. Mater.*, 2011, **10**, 823–837.